01 Jan 2024

A Review of Current Safe Distance Calculations and the Risk of Mild Traumatic Brain Injury

A. R. Loflin

C. E. Johnson
Missouri University of Science and Technology, johnsonce@mst.edu

Shock Waves
https://doi.org/10.1007/s00193-024-01197-y

ORIGINAL ARTICLE

A review of current safe distance calculations and the risk of mild traumatic brain injury

A. R. Loflin[1] · C. E. Johnson[1]

Received: 25 January 2023 / Revised: 19 July 2024 / Accepted: 21 July 2024

Abstract

Explosive breaching is a tactic operational professionals use to gain rapid entry and tactical advantage. This tactic exposes individuals to repeated low-level blasts (LLB), overpressure exposure generally occurring from user-directed munitions. The experimentation described in this paper highlights the need for further research into implementing explosives in tactical situations, specifically in confined areas, and the effects on individuals exposed. While current safety calculations predict peak pressures from an open-air detonation, this study incorporates the impulse of the total explosive event in a confined space. Sixteen explosive events were conducted to measure peak overpressures of the total duration of the event using pencil probes and flush mount-type sensors. These pressure sensors measured detonations at distances greater than or equal to the calculated minimum safe distances (MSD). The study compares these data with the Hopkinson–Cranz scaling law, the Weibull formula, and Kingery–Bulmash (KB) predictions. Additionally, a scaled mouse-to-human model for developing mild traumatic brain injury (mTBI) using pressure vs. impulse (*P–I*) graphs demonstrates areas of concern in the collected data. Results show that at distances exceeding the MSD, with personal protective equipment (PPE), and at pressures lower than those considered safe, mTBI is possible. Peak overpressures were measured to be 2.5 times higher than safety thresholds and impulses as high as 274 kPa ms. Confined area detonations produced 1.2–1.4 times greater pressures than open-air detonation measurements. Individuals who undergo breaching training will likely experience multiple exposures of this nature throughout their career, often occurring in rapid succession.

Keywords Explosive breaching · Traumatic brain injury · Confined detonations · Scaled distance · Explosive overpressure · Explosive impulse · Low-level blasts

Abbreviations

CODI	Combat ordnance diagnostic instrument
DAS	Data acquisition system
KB	Kingery–Bulmash
LLB	Low-level blast
mTBI	Mild traumatic brain injury
MSD	Minimum safe distance
NEW	Net explosive weight
PETN	Pentaerythritol tetranitrate
P–I	Pressure vs. impulse
PPE	Personal protective equipment
PTSD	Post-traumatic stress disorder
R.E.	Relative effectiveness
VOD	Velocity of detonation

Communicated by R. Banton, T. Piehler, and R. Shoge.

✉ C. E. Johnson
Catherine.Johnson@mst.edu

A. R. Loflin
Arl39w@mst.edu

[1] Mining and Explosives Engineering, Missouri University of Science and Technology, 290 McNutt Hall, Rolla, MO 65409, USA

1 Introduction

In breaching events, explosives are only one of the many hazards an entry team will encounter. The primary hazard is the possibility of armed combatants on the other side of the entryway. In such cases, breachers often employ risk vs. reward calculations to decide if bringing the distances down between the assault team and the entry point could result in tactical superiority. Conversely, being too close to an explosion risks injury to the assault team, reducing capabilities and potentially causing further injury upon entry [1]. These factors are

Published online: 24 August 2024

at the forefront of a breacher or assault team leader's mind. At the same time, the possibility of barotrauma being inflicted, not only that day but in the weeks and months to follow, is often a secondary concern [1]. In training, breaching teams are exposed repeatedly to overpressure that can lead to barotrauma [1–4]. This training involves multiple breaches a day for many consecutive days, multiple times a year, depending upon the specifics of the training. Over a career, this can have an additive effect, leading to cognitive, sleep, and attention issues [2, 3, 5]. It has also been linked to more severe effects such as traumatic brain injury (TBI), depression, and post-traumatic stress disorder (PTSD) [2].

Tools to help calculate the minimum safe distance (MSD) are available to breachers. However, ultimately, it is up to the breacher to make the final call on where to place a team, what charges to use, and any other variable that could lead to the success or failure of a breach. These tools have been developed and fielded for decades and have been successful in their tactical use. However, as knowledge of TBI mechanisms expands, these methods have come under scrutiny and the search for improved tools has commenced, particularly the validity of MSD calculations in interior/confined settings [1, 2].

MSD calculations are crucial to any breaching plan and serve as critical safety guidelines [1]. Many breachers and assault teams will add additional distance onto the calculated safety distance. A typical thought process is "MSD plus one foot," rounding up for safety. While relatively easy to accomplish in an open-air environment, it can be impractical in confined spaces. If available, a corner or barricade will be used as a safety measure; however, a breacher or team may deem it necessary to be as close to the detonation as possible or be limited in choices [1]. In such cases, it is critical to predict pressure and distance accurately. An anecdotal survey conducted by the authors from multiple sources with breaching capabilities found the K-factor and Weibull formulas to be the most prevalent tools, specifically when applied to confined spaces.

The K-factor calculation, a scaling factor based on the Kingery–Bulmash relationship [6, 7] and the Hopkinson–Cranz scaling law [8–10], was developed in the mid-twentieth century based on large-scale explosive testing in an open environment [11]. Its development did not have breaching in mind, but rather the destruction of structures and equipment from large-scale explosions. It also does not account for the various risk factors present in breaching, such as reflected overpressure or fragmentation [12]. Instead, it calculates the peak incident pressure, also known as side-on pressure, in pounds per square inch (psi) at a given distance. The most common derivation of the equation predicts a distance from the detonation where the peak pressure is no higher than four psi (27.5 kPa), a level considered safe with hearing protection. This equation derivation represents the most common application and is likely the main calculation used in commercial products provided to some of the surveyed operational professionals. It should be noted that a subset of individuals surveyed using the calculators exclusively did not understand the source of the outputs of the supplied calculators. Due to operational security considerations, this paper will not publish the exact equations currently fielded.

The Weibull formula [13] was initially derived to help design explosive chambers for nuclear detonation simulators. The formula became a tool for determining pressure in an entire volume after an explosion by breachers, likely due to the formula's incorporation into a computer program to predict damage to aircraft interior structures in 1972 [14] and later adopted as a safety measure. Like the K-factor equation, the Weibull formula does not account for reflected overpressure, complex geometries, or other hazards.

This study compares the calculations used in interior breaching with experimentally collected airborne shock data. The outputs from both laboratory-grade sensors and a field-grade wearable sensor are compared with the Kingery–Bulmash (KB) predictions [6] to assess each method's ability to accurately predict the peak overpressure experienced in an interior or close space breaching scenario. The results are also applied to pressure vs. impulse (P–I) graphs, which represent the relationship between pressure and impulse and are often used to estimate potential damage [15]. These graphs provide a better picture of the conditions that can lead to overpressure-induced mTBI. The calculations presented aim to reduce the probability of injury to individuals by ensuring they are positioned at a distance and in an environment where they would encounter peak pressure of less than 27.5 kPa for all orientations and pressure types [16, 17]. This threshold pressure is an accepted level below experimental measurements of 34.5 kPa that equates to the threshold for eardrum damage [18] regardless of orientation.

2 Methodology

2.1 Charge construction

An interior strip charge provided the explosive pressure for all 16 detonations to evaluate the effectiveness of the K-factor and Weibull calculations. The charge consisted of a 1.9 × 30-cm strip of 3-mm-thick PRIMASHEET 1000 flexible explosives [19], backed by a 1.27-cm strip of rubber matting [20] as shown in Fig. 1. The flexible explosives consist of 63% PETN, 9% nitrocellulose, 27% plasticizer, and 1% taggant, with a detonation velocity of 7.1 km/s [19]. The term detonation is used throughout this manuscript to describe the energetic reaction present. While the research team took no direct measurement of the velocity

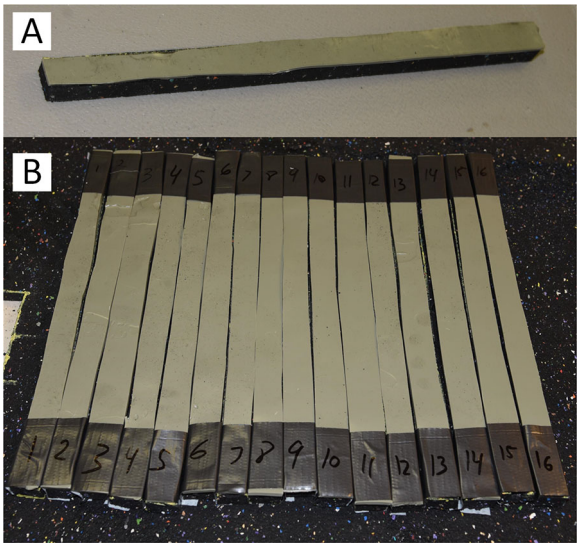

Fig. 1 Interior strip charge construction. Image **A** represents typical charge construction with a single layer of flexible explosives on top of a 1.27-cm-thick strip of rubber matting. Image **B** represents all charges used in the testing described in this paper

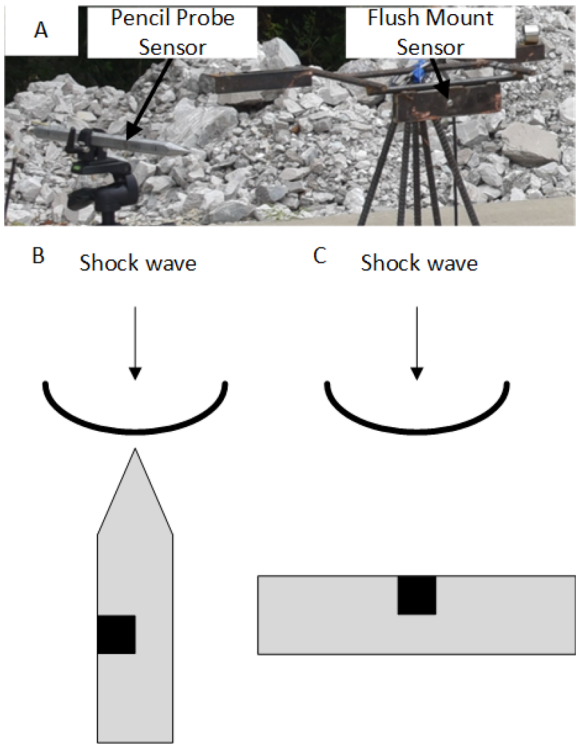

Fig. 2 Example of sensor orientation and side-on and head-on wave measurement principles. Image **A** shows the co-located pencil probe-type (left) and surface mount (right) pressure sensors, with indicators for the actual sensor positions in the test apparatus. Schematic **B** shows that the pencil probe sensor, parallel to the blast wave streamline, collects side-on pressure data. The surface mount sensor, perpendicular to the blast wave streamline, measures head-on pressure data, as shown in schematic **C**. The black-shaded areas of schematics **B** and **C** represent the sensor element position and orientation with respect to the direction of travel of the shock wave

of detonation (VOD), initiation energy sufficient to detonate the primasheet was used, and there was no evidence of deflagration or combustion present.

Charges contained 30 ± 0.5 g of flexible explosives, with priming wells carved out of the rubber backing for placement of an electric initiator. Two net explosive weights (NEWs) were calculated. One used a field method that calculated the sheet explosives' volume and converted that volume's grain weight to pounds of TNT: NEW$= \frac{L \times W \times T \times 15.4 \times 1.66}{7000}$, where L is length, W is width, T is thickness, all in inches, 15.4 is a conversion factor for grams to grains, and 1.66 is the relative effectiveness (R.E.) factor for the flexible explosives. This method produced a NEW value of 0.099 lb of TNT (44.9 g of TNT). This field method is purposefully conservative. A 1.66 R.E. factor is the highest factor found in any explosive reference manual and is used to establish a standard across military and police units. The second method was based on the 30-g weight and the constituent components of the flexible explosives, PETN, nitrocellulose, plasticizer, and taggant, resulting in a NEW of 0.08 lb of TNT (36.3 g of TNT). This method would be closer to lab calculations for exactness. All charge construction, safe distance calculations, and other breaching-orientated testing considerations were conducted by a trained breacher ensuring relevance to military practices and the proper applications of MSD calculations.

2.2 Instrumentation

A Hi-Techniques Synergy data acquisition system (DAS) [21] was used to record pressure data. Five PCB Piezotronics Model 137B23B pencil probe-type pressure sensors [22] collected side-on overpressure measurements. Three PCB Piezotronics Model 102B15 flush mount pressure sensors [23] were co-located with the first three pencil probes to measure head-on pressure. Side-on pressure is "the pressure collected parallel to a blast wave streamline" [24], while head-on pressure is measured with the sensing element perpendicular to the blast wave streamline. An example of the co-located sensors and their concept of operation is shown in Fig. 2.

The custom-built combat ordnance diagnostic instrument (CODI) simulates human exposure to explosive shock waves. The CODI was outfitted with personal protective equipment, including a helmet and plate carrier with steel ballistic inserts, as shown in Fig. 3. A wireless, body-mounted, wearable sensor (B3 wireless pressure sensor [25]) was attached to the forward-facing section of the plate carrier. One PCB Piezotronics 102B18 [26] and four embedded PCB Piezotronics 102B15 [23] flush mount pressure sensors were used correlating with the CODI's left eye (2), forehead (3),

Fig. 3 CODI with helmet and plate carrier. A B3 wireless pressure sensor is mounted on the plate carrier's front

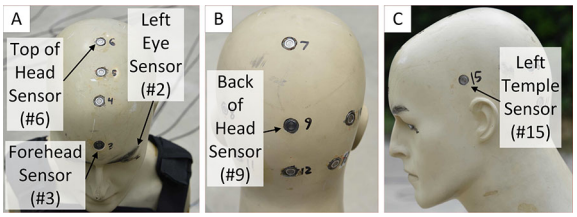

Fig. 4 The CODI sensor placement. Image **A** shows the locations of the forehead, left eye, and top-of-head sensors. Image **B** shows the location of the back of the head sensor. Image **C** shows the location of the left temple sensor. All sensors, except the forehead and left eye sensors, are located under the helmet donned on the CODI. The forehead sensor is partially exposed, and the left eye sensor has no shielding from the shock wave

top of the head (6), back of the head (9), and left temple (15) [23]. Sensor placement is shown in Fig. 4.

2.3 Test setup

Figure 5 shows that the strip charge is suspended in air, and its midpoint is 1 m from the ground. This height simulates the height of the average doorknob.

The first pencil probe and flush mount sensor were placed directly before the strip charge at 2.54 m. This MSD calculation uses the NEW determined by the field calculations. As no shielding is available in this scenario, a K-factor of 18 provides a distance that would experience less than 27.5 kPa. This calculation has an inherent safety feature, as all explosives are given a 1.66 R.E. factor. From this point forward, these sensors will be referred to as Side-on 1 and Head-on 1. The distances for the fourth and fifth pencil probes match Side-on 1 with different angle placements. These sensors are henceforth called Side-on 4 and 5.

The second pencil probe and flush mount sensor, Side-on 2 and Head-on 2, were placed at the MSD and calculated by the weight of the explosive components of the flexible explosives charge. They were placed exactly 25.4 mm closer to the charge at an offset angle greater than 9 degrees so as not to interfere with other sensor readings [27, 28]. The calculated MSD using the exact weights of the charge's explosive components was 2.33 m using the K-factor equations.

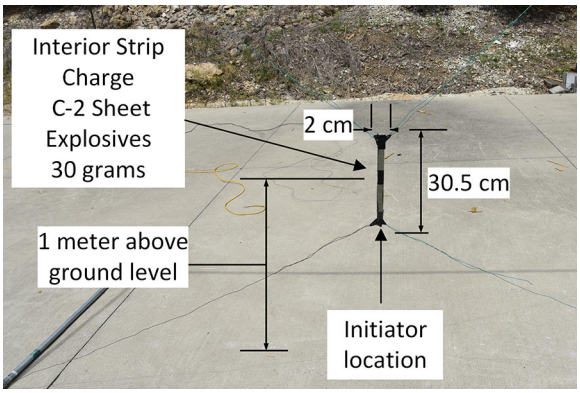

Fig. 5 Test setup for suspended strip charges in an open-air environment. The strip charge is suspended with its center of mass 1 m from the ground. The 2 × 30.5-cm strip charge consisted of 30 g of flexible explosives. Once initiated, the shock wave travels through the charge from the initiation point, designated in the figure at the bottom of the suspended charge, along the length of the strip charge until all energetic materials have been consumed in the explosion

The CODI's sensor 3, the forehead, was placed precisely 2.74 m from the charge. This distance simulated the MSD+1-foot operational idea, using the field calculations likely used in training and operational situations. For the open-air detonations, the CODI was rotated from head-on to a left ear-facing orientation; this was not repeated for the enclosed environment testing. Each angle recorded was for a single explosive event, and repetitions were not carried out at each orientation.

A final sensor pairing was placed at 3.96 m from the charge, Side-on 3 and Head-on 3. This placement compares their data to KB predictions [6] after testing and provides a data point well past calculated MSD. All sensor positions and distances remained the same throughout testing and are provided in Fig. 6.

2.4 Open-air test

Four detonations were performed on a concrete pad in an open-air environment at 24.96 °C and an atmospheric pressure of 98.88 kPa. These detonations form a baseline for comparison to existing MSD calculation methods. Figure 7 depicts the basic setup of the four open-air detonations.

2.5 Confined space tests

An underground limestone mine was chosen for the interior detonation test series due to the mine walls' complex geometry and existing infrastructure for explosive testing. The inside of the underground test area could easily simulate the interior of a brick or stone structure, close-quarter

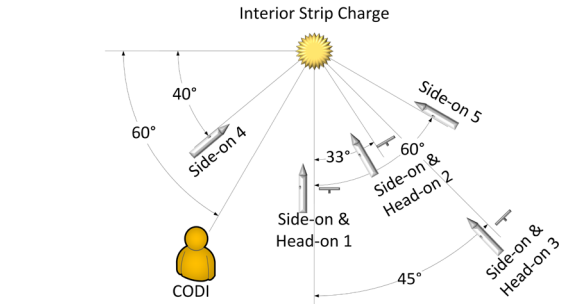

Field MSD: 2.54 m
Side-on and Head-on 1
Side-on 4
Side-on 5
Weight MSD: 2.34 m
Side-on and Head-on 2
CODI: 2.74 m
Kingery-Bulmash: 3.96 m
Side-on and Head-on 3

Fig. 6 Test setup and sensor placement. Sensor placement indicated in the figure remained constant throughout testing

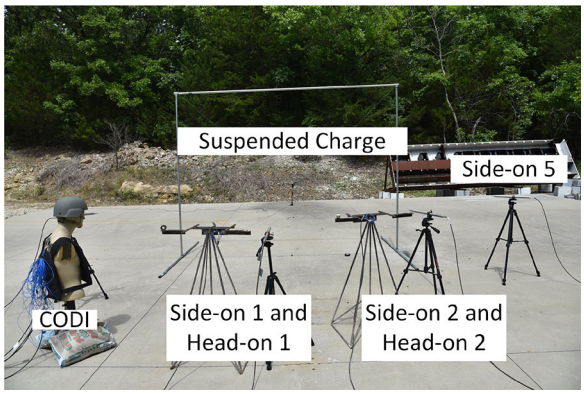

Fig. 7 Open-air detonation test site. The figure depicts the setup of the open-air detonation testing area with sensors. The Side-on 3 and Head-on 3 sensors are not shown as they are out of frame, and the Side-on 4 sensor is behind the CODI in this image

alleyways, or cave complexes where breaching may occur. Four different sites were used within the test area to evaluate different scenarios. Figure 8 shows the locations of each test area within the experimental mine complex.

All sites were placed near the overhead exhaust vent and fan, allowing accessibility to the cabled pressure sensors from the DAS located on the surface. Site 1 comprised a flat concrete wall and the open geometry of the adjacent pathways. Site 2 was a corner formed by the mine walls, and Site 3 was placed close to Site 2 on the mine wall. These sites allowed for differing geometries near each other. An entryway was chosen for Site 4 to mimic operational conditions, allowing the pressure sensors to measure the effects of the doorway reflecting pressure realistically. Sensors Side-on 3 and Head-on 3 were placed inside the entryway to collect shock wave data inside the breaching area. In contrast, all other sensors

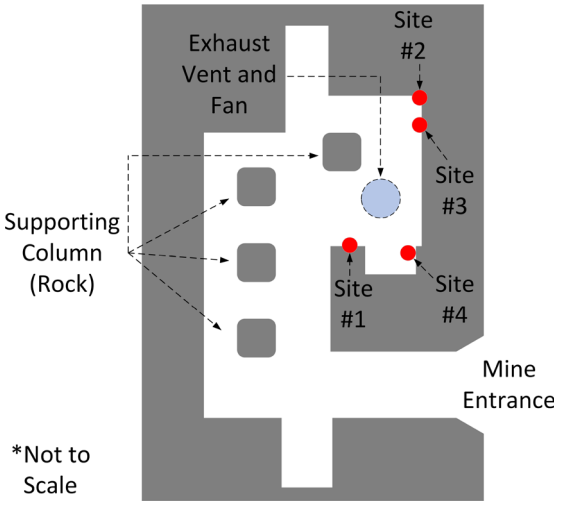

Fig. 8 Layout of confined space testing sites. The test site included an overhead exhaust vent and fan, multiple supporting rock columns, and multiple alcoves, providing a test area with complex geometry

were placed outside of the entryway to collect data on the area where a breaching team might stand.

3 Results and analysis

Four underground scenarios were compared to an open-air control test at various standoff distances to evaluate the applicability of different MSD calculations in a confined space. Figure 9 shows the peak pressure results of all sensors in the test series.

For an MSD calculated with the K-factor formula, the maximum pressure experienced by an individual should be no more than 27.5 kPa; this proved an accurate calculation for all pencil probes in the open-air detonation test series (detonations 1–4). In the confined space detonations, this also was generally a reasonable calculation for the pencil probe sensors placed away from the mine wall. These data validate the calculation since side-on measurements from large-scale explosive charges in open-air detonations were used to formulate the K-factor equations.

The trend of staying below the predicted pressure does not hold for the flush mount sensors that measure head-on pressure. As mentioned in the test setup section, Head-on 1 and 2 sensors are at an MSD calculated according to their NEW, 2.54 and 2.34 m, respectively. Head-on 3 is 3.96 m from the charge and is the only sensor that registers peak pressures below the 27.5-kPa threshold; this is true for both the open-air and the confined space detonations. The wearable sensor data are displayed in Fig. 9b alongside the flush mount sensor data. The sensor fluctuated between 22 and 30 kPa for peak pressure in open-air detonations. In the confined space

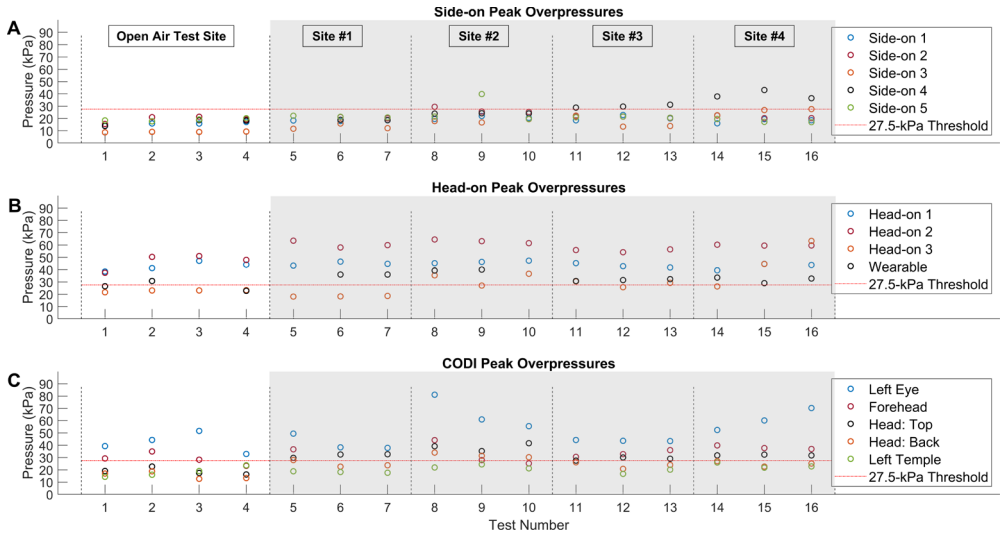

Fig. 9 Peak overpressures for all sensors used in testing. Graph **A** displays the results of pencil probe sensors. Graph **B** displays the results of all flush mount pressure sensors and the wearable sensor. Graph **C** displays the results of all flush mount pressure sensors used on the CODI. The dashed red line in all three images indicates the 27.5-kPa threshold for hearing damage. The shaded area of the graphs indicates tests conducted in confined areas

detonation testing, the sensor registered above 27.5 kPa for all tests with a peak of 40 kPa.

The CODI results also show a discrepancy with this calculation. Recall that the CODI is 2.74 m from the charge, an additional 20 cm past the calculated MSD. While some sensors read below the 27.5-kPa level, others are elevated as the orientation of the CODI changes relative to the charge. During the open-air detonations, the CODI begins facing the charge, and with each subsequent detonation, the CODI is rotated until its left ear faces the charge at shot 3. This behavior is likely due to the helmet protecting some sensors, specifically the left temple and others under the helmet, from the direct exposure to the shock wave.

In contrast to the sensor under the helmet, others were exposed, such as the left eye and forehead. Orientation of the sensors to the detonation also affected the pressure experienced, as sensors will experience a shift from side-on to head-on orientation between shots. If a given sensor is in a head-on orientation, it will experience more significant reflected (head-on) pressure as the shock wave interacts with its entire surface area while reflecting off in the opposite direction. If that same sensor were parallel (side-on) to the direction of the shock wave propagation, it would only experience the initial rise as the wave passes. Head-on and side-on orientations are illustrated in Fig. 2. This phenomenon is known and can inflict injuries, especially in the ear and lungs, as head-on orientations during blast exposures result in more significant energy transfer into the pressure-sensitive organs [29]. Shot 4 returned CODI to its original orientation; all subsequent shots were with the CODI facing the charge. This movement provides data for comparing the fluctuations in the head-on pressure data between testing events in the confined area detonations. It should be noted that the wearable sensor's peak pressures track closely with the CODI forehead and top-of-head sensors.

As shown in Fig. 9, once the test series moved into a confined area, even side-on pressure peaks were challenging to predict with the K-factor formula. When calculating these MSDs, head-on pressure is not a consideration due to how the formula was originally derived. It can also be observed that pressure readings can vary noticeably between detonations at the same site. This variability is likely due to slight changes in the placement of the charge in conjunction with the complex geometry of the mine walls; even the slightest movement left or right may change the angle at which the shock wave reflects from the wall face. This indicates that the predictive power of these equations is only reliable in non-confined environments.

Compared to the KB predictions, the side-on pressures in the open-air detonations are close to the predicted values. Deviations from the predictions occurred when the sensors moved from the open-air test site to the confined space test area. Head-on pressures were consistently higher throughout the experimentation and close to the predicted values in the open-air environment. The CODI does not follow this trend, with side-on pressure readings higher than predicted but head-on pressures in line with calculations. The wearable sensor's peak pressure was lower or directly in line with the KB predictions, but its initial impulse calculations were more than double the predictions. Results of the KB

Table 1 Comparisons between Kingery–Bulmash predictions and averaged sensor data

Distance (m)	Orientation type	Predicted overpressure (kPa)	Predicted impulse (kPa ms)	Average measured overpressure (kPa)	Average calculated initial impulse (kPa ms)	Average calculated total impulse (kPa ms)
2.53	Head-on	38.3	20.3	42.70_o 44.23_c	8.66_o 10.1_c	10.9_o 103_c
	Side-on	17.9	10.4	17.19_o 23.15_c	8.13_o 16.6_c	9.67_o 115_c
2.33	Head-on	41.1	20.8	46.65_o 59.71_c	9.65_o 12.6_c	13.1_o 106_c
	Side-on	19.1	10.6	19.23_o 22.52_c	9.05_o 12.6_c	11.5_o 105_c
2.75	Head-on	33.7	18.6	24.66_o 33.12_c	12.2_o 28.1_c	15.1_o 176_c
	Side-on	15.79	9.58			
3.96	Head-on	20.2	2.90	22.74_o 31.10_c	6.56_o 16.3_c	7.56_o 109_c
	Side-on	9.65	1.37	9.01_o 18.32_c	6.89_o 20.4_c	7.42_o 123_c
Wearable	Head-on	33.7	18.6	26.67_o 34.10_c	14.7_o 46.7_c	n/a n/a

The table compares calculated KB predictions to averaged sensor measurements. "$_o$" represents averaged measurements of open-air detonation; "$_c$" represents averaged measurements of confined area detonations. The averaged CODI measurements are for all five sensors used on the CODI. The wearable sensor data are added at the bottom of the table for comparison. Due to the predetermined save duration, only initial impulse was possible

Table 2 Results of Weibull's calculations

Open air	n/a
Site 1	12.06 kPa
Site 2	7.78 kPa
Site 3	7.78 kPa
Site 4	12.34 kPa

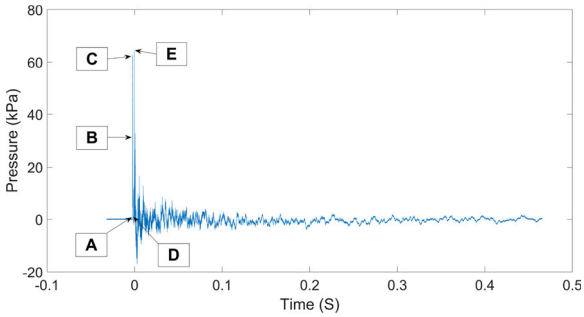

Fig. 10 Waveform of Head-on 2 sensor, shot 8. Without zooming in, it is difficult to differentiate between the initial peak pressure and the actual peak pressure of the event. Point A shows the initial arrival of the shock wave. Point B shows the initial rise in pressure as the shock wave encounters the sensor. Point C shows the initial peak pressure. Point D shows the first instance when the pressure enters the negative phase, and Point E indicates the actual peak pressure of the measurement

calculations as compared to averaged sensor data are shown in Table 1.

For Weibull's equation, sites were imagined to be simple boxes for their volume measurements, ignoring openings to other chambers, vents, and variations in face walls. Since the entirety of the underground complex's volume was of greater magnitude than the simple boxes imagined, the equation would predict near zero pressure with the ratio of volume to explosive weight seen in the Weibull equation being magnitudes larger. Table 2 presents the calculated pressures expected in each volume, which are much lower than those seen through experimentation.

It is evident that Weibull's equation is not an adequate calculation for prediction, and even breaching schools note that this calculation was never intended for use in breaching [30].

While the output of all sensors shows pressures that exceed the 27.5-kPa limit, it does not exceed it to the point of moderate or severe injury found in literature [16, 18, 29, 30]. A few pressure sensors approach 103.4 kPa, the level attributed to 50% eardrum damage in a population of humans [16], but all detonations measured were below this threshold. An evaluation of published data showed that mTBI could develop at pressures well below that in animal models [31–33]. A proposed way of equating animal test results to a human model is to scale the results with the considerations of the protective structure to brain mass ratio [34].

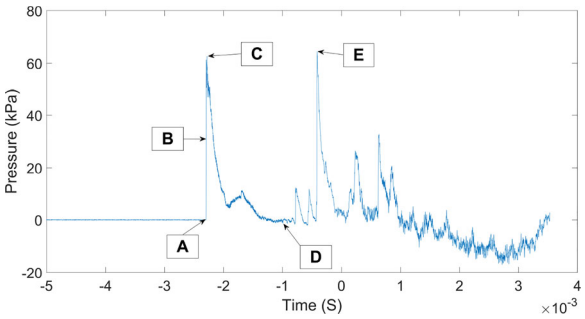

Fig. 11 Magnified view of the waveform from Head-on 2 sensor, shot 8. It is noticeable that the initial peak has a lower magnitude than the reflected pressure wave that follows it. Point A shows the initial arrival of the shock wave. Point B shows the initial rise in pressure as the shock wave encounters the sensor. Point C shows the initial peak pressure. Point D shows the first instance when the pressure enters the negative phase, and Point E indicates the actual peak pressure of the measurement. With this magnified view, a secondary shock wave can be seen between the initial peak at Point A and the peak pressure at Point E

Most current research is in the open field or shock tubes designed to mimic the simple exponential decay of the Friedlander waveform [31, 35]. Calculating the initial impulse is standard practice, but head-on pressures can exceed the initial peak pressure in confined space scenarios, as shown in Fig. 10. Also shown in the figure are multiple reflections considerably above ambient pressures throughout the event. A closer inspection of the first six milliseconds of the event, shown in Fig. 11, shows the lost data if the initial impulse alone is calculated. To this end, the initial impulse and the total impulse for the entire duration of an explosion were calculated.

For the initial impulse, a pressure threshold was used in calculations when the pressure first rose above and fell below 0.7 kPa. The area under the pressure curve between those two points was then calculated using the trapezoidal numerical integration method with MATLAB [36]. The results of this integration are shown in Fig. 12.

All initial impulses measured from the pencil probes were below 28 kPa ms, and the initial impulses measured from the flush mount sensors were below 25 kPa ms for both open-air and confined area tests. The wearable sensor's maximum initial impulse in the open air was 17 kPa ms, considerably lower than its confined space maximum of 54 kPa ms and less than half of its minimum at 36 kPa ms. The wearable sensor on the front-facing plate of the CODI's body armor maintained a higher initial impulse measurement than the flush mount sensors for all confined area detonations. The CODI results showed more variation due to location than other sensors, with a maximum of 71 kPa ms occurring at Site 2 of the underground test area. Interestingly, this pressure was captured by the sensor on top of the CODI's head, protected from the shock waves by the helmet. This is possibly due to the helmet underwash effect [37–39]. Site 2 registered the highest measurements for all sensors on the CODI, likely due to the increased reflected waves from the corner junction of the rock wall.

Calculated initial impulses were then plotted onto a *P–I* graph, commonly used to visualize damage thresholds. These data points are compared to collected data known to have induced mTBI in animal studies [31, 40–42]. The animals were placed 3 m from a 350-g charge of Composition C-4 and exposed to the overpressure and then subjected to behavioral assessments, histological observations, and biochemical analysis [31]. The data points were scaled to a human model using Jean et al.'s scaling law [34]. As Jean et al. mentioned, this scaling law predicts that humans are more susceptible to pressure-induced brain injuries, requiring approximately 70% of the pressure. As impulse was not considered an element of the scaling law, measured impulses are used for the *P–I* graph. These data only incorporate published papers that reported pressure and impulse values and do not imply that mTBI is impossible beyond these levels.

Figure 13 shows the *P–I* graph. The upper right quadrant of the graph is bounded by the averaged measured impulse from the animal study and average pressure value indicating mTBI in mice scaled to humans, showing conditions where mTBI may occur [34]. It is unsurprising to see few data points in this region when only the initial impulse is considered. It should be noted that of the data in this region from the confined space explosions, the most concerning data are from the sensors under the CODI's helmet and left eye, though the sample size is limited to three data points.

For the total impulse of the event, the same threshold of 0.7 kPa was used, and the initial rise above this point was set as the beginning of the numerical integration. The end of integration occurred when the pressure fell below this point for the final time in the recorded event. These parameters allow for all reflected waves to be included. This is significant as the initial and total impulses vary greatly. While the initial impulse suffices for open-air detonations due to limited reflections, energetic events indoors can have reflections greater than the initial side-on wave. Figure 14 demonstrates the difference between open-air and confined area detonations and the resulting pressure wave reflections with a side-by-side comparison of the same sensor in each environment.

The results of calculating total impulse change little for the first four detonations, which were conducted in an open-air environment and had relatively few reflected shock waves. Charges detonated in enclosed environments show a more significant increase in impulse when all reflected waves are considered. As shown in Fig. 15, total impulse moves almost all the points well above the measured impulse line that indicates mTBI in mice. Almost all pencil probe measurements were below the 27.5-kPa threshold, with the outliers close to the mine walls. Conversely, virtually all the head-on data

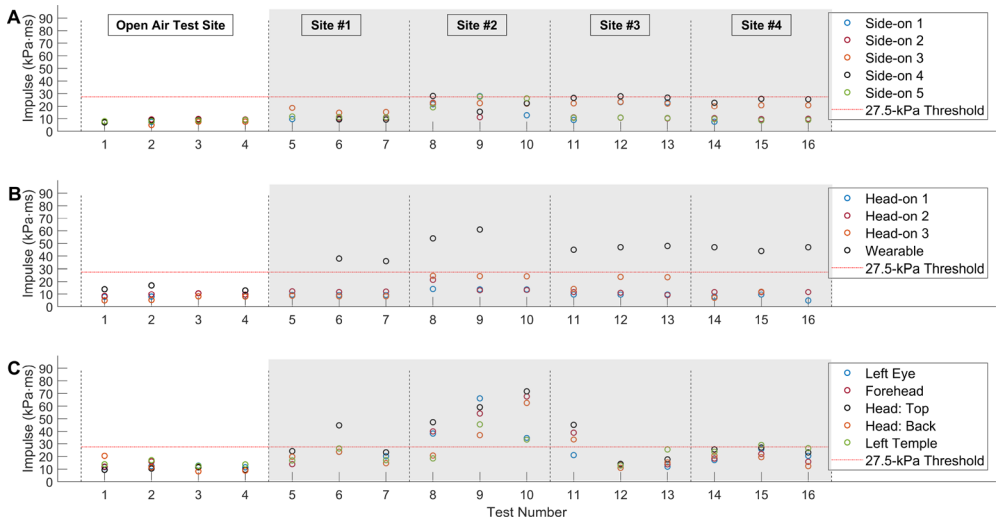

Fig. 12 Initial impulse for all sensors. Graph **A** displays the results of pencil probe sensors. Graph **B** displays the results of all flush mount pressure sensors and the wearable sensor. Graph **C** displays the results of all flush mount pressure sensors used on the CODI. The dashed red line in all three images indicates the 27.5-kPa threshold for hearing damage. The shaded area of the graphs indicates tests conducted in confined areas

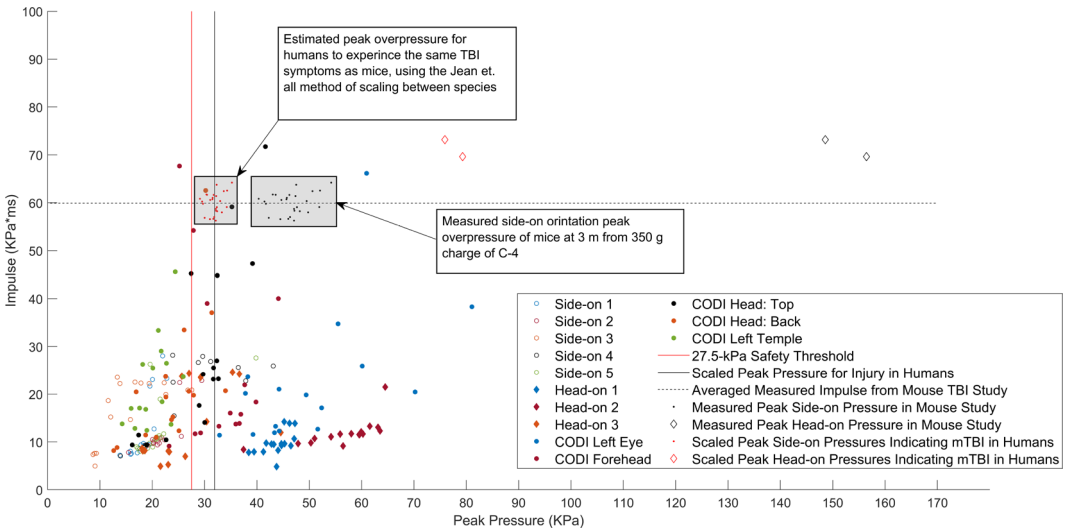

Fig. 13 Initial impulse *P–I* graph for all sensors. The vertical black line represents the average peak pressure scaled from experimental animal test studies indicating mTBI in humans. The horizontal black dashed line represents the average measured value of impulse that indicates mTBI, based on data collected in the literature that provided enough information to know both overpressure and impulse. The vertical red line indicates the 27.5-kPa pressure value the MSD calculations intended to obtain

points are above the threshold, except Head-on 3, which was 1.42 m further away from the explosion than the MSD. The CODI showed some of the highest collected impulse and peak pressure measurements, with calculated MSDs and PPE donned on the CODI. The sensor readings under the protective helmet are of particular interest, with a majority near the same peak pressure as the mouse data scaled to humans and 4 to 5 times the impulse.

A point of concern these data highlights is that while these data points are on the lower end of what could be considered an mTBI threshold, breaching operations may have multiple confined space detonations in a short period, which could lead to numerous chances for an individual to be exposed to overpressures and impulses that can cause mTBI and compounding effects of repeated LLB [3, 24, 43, 44]. This short period could be a matter of minutes for multiple detonations on one engagement or a matter of

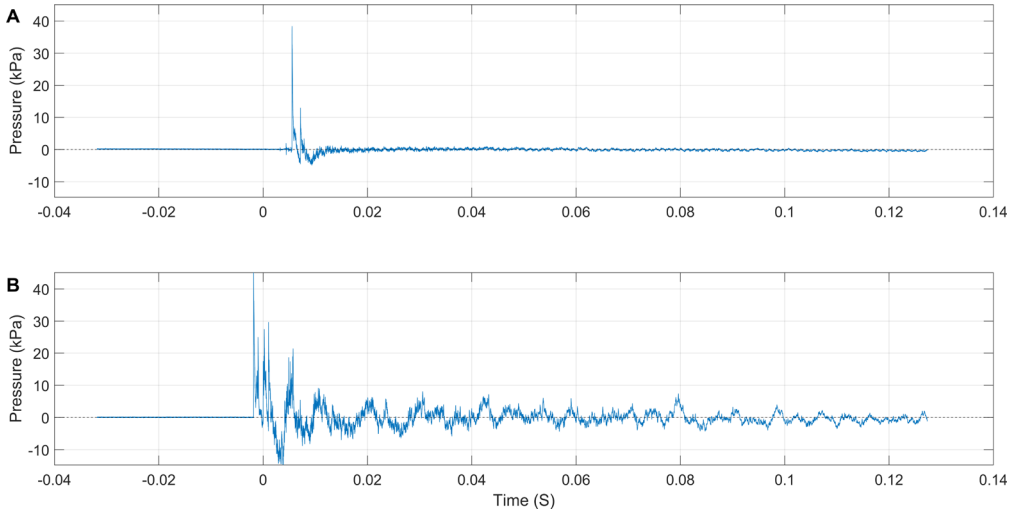

Fig. 14 Comparison between open-air and confined space detonations. Image **A** depicts the results of the open-air detonation of shot 1. Image **B** depicts the results of the confined space detonation of shot 8. Note that the amplitude and duration of pressure change in image **B** are greater than image **A**'s

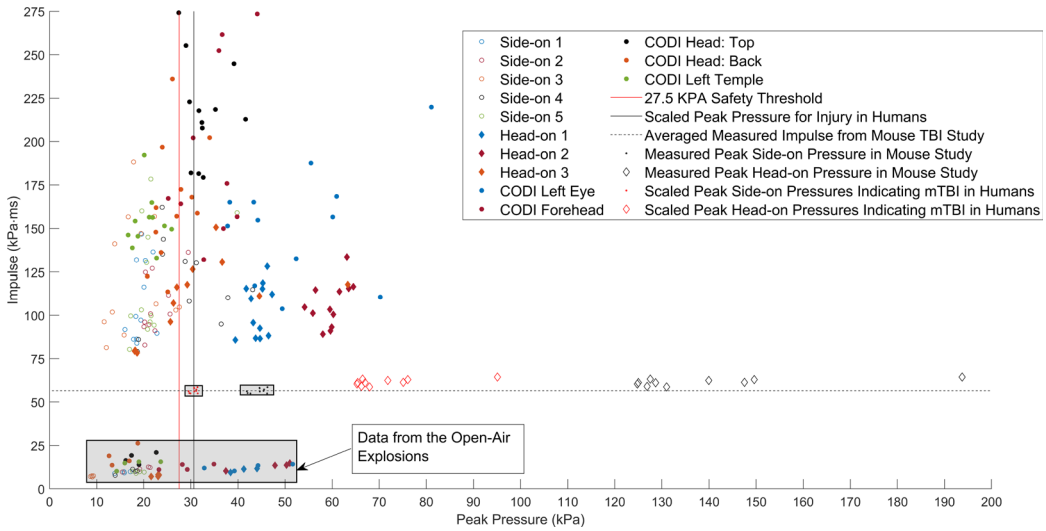

Fig. 15 Total impulse *P–I* graph for all sensors. The vertical black line represents the average peak pressure scaled from experimental animal test studies indicating mTBI in humans. The horizontal black dashed line represents the average measured value of impulse that indicates mTBI, based on data collected in the literature that provided enough information to know both overpressure and impulse. The vertical red line indicates the 27.5-kPa pressure value the MSD calculations intended to obtain. Due to manufacturer data outputs, wearable sensor data are omitted from total impulse calculations

hours and days for numerous engagements. Outside of operational environments, a high training tempo may also provide an opportunity for exposure to these types of explosions [4].

4 Conclusion

This study evaluated the effectiveness of the minimum safe distance calculations in enclosed environments and compared experimentally collected data to published conditions known to have caused mTBI in animal studies. From the experimental results presented with 30-g charges in a confined environment, air overpressure and impulse levels were higher than published literature citing the onset of mTBI. The K-factor method for predicting safe distance is based on side-on pressure measurements of large-scale explosions in an open area and does not account for reflected pressure waves. While accounting for the volume of an enclosed space, the Weibull equation did not provide accurate representations of the pressure experienced in the explosions. The KB predictions calculated reflected overpressure, but only in an open-air environment, and none of the equations evaluated considered impulse. Data collected in this experimentation

resulted in peak pressures as high as 81 kPa at distances greater than MSD, 2.9 times greater than the recommended safe limit. The total impulse calculated from this experimentation was as high as 274.16 kPa ms under the CODI's helmet, 4.85 times higher than average measured impulses that have indicated mTBI in mice [40, 41].

Results provided in this manuscript show that commonly used equations cannot accurately predict safe distances or expected overpressure values in enclosed environments. While this is already well known in the breaching field, and many of these equations come with disclaimers noting that it is up to the individual on the ground to use their best judgment [30], these tools are still taught and not replaced with a method that can provide a definitive safe option that meets the breachers' needs. Furthermore, even without signs of physical injury and with the use of current PPE, mTBI can still be possible, as shown by pre-clinical research [40–42] and represented in the *P–I* graphs.

Additional testing is needed to gather data on small explosive charges in confined areas, repeated exposure to these charges, and the effects of complex geometries affecting the tools currently fielded. Future explosive testing must include impulse data, including all reflected pressure waves. These data will expand the understanding needed to develop new formulas, techniques, and PPE that will help prevent mTBI and other injuries in the future. A better understanding of the mechanics of TBI is also needed to move forward with improvements to breaching safety and other tactical explosives use, with an emphasis on the development of an accurate human model for neurotrauma.

Any methods developed must consider the total impulse of an explosive event rather than peak pressure or initial impulses alone. Pressure and total impulse comparisons, as shown in the *P–I* graphs, are one such method that should be further developed. *P–I* calculations can be an early indicator of possible mTBI exposure. These indicators will help identify individuals who need to be removed from an environment where they may be exposed to repeated LLB [3], lowering their risk of incurring or exasperating an already existing injury.

Acknowledgements We want to express our gratitude to Ian McKeown, Michael Newcomer, and Trevor Taormina for their previous research and testing that paved the way for this current experimentation. We also thank Rachel Bauer, Cody Thomas, Emily Johnson, and Michael Koenig for their valuable contributions to the experimentation process. Lastly, we appreciate Amy Cooper-Loflin for her diligent review and editing of the manuscript. This work was funded by the Johnson Grad Group internal funds at Missouri S&T.

Declarations

Conflict of interest The authors declare that they have no conflict of interest. The authors did not receive support from any organization for the submitted work. There is no affiliation, either direct or indirect, between the authors and the sensor manufacturers referenced in this document.

References

1. Murphy, J.: Special Ops has a broken culture with explosive breaching that can lead to TBIs. https://www.sofsupport.org/special-ops-has-a-broken-culture-with-explosive-breaching-that-can-lead-to-tbis (2020). Accessed 19 Nov 2022
2. Stewart, W., Trujillo, W.: Modern Warfare Destroys Brains: Creating Awareness and Educating the Force on the Effects of Blast Traumatic Brain Injury. Harvard Kennedy School, Belfer Center for Science and International Affairs (2020). https://www.belfercenter.org/publication/modern-warfare-destroys-brains
3. Ravula, A.R., Das, T., Gosain, A., Dolalas, T., Padhi, S., Chandra, N., Pfister, B.J.: An update on repeated blast traumatic brain injury. Curr. Opin. Biomed. Eng. **24**, 100409 (2022). https://doi.org/10.1016/j.cobme.2022.100409
4. McEvoy, C.B., Crabtree, A., Powell, J.R., Meabon, J.S., Mihalik, J.P.: Cumulative blast exposure estimate model for special operations forces combat soldiers. J. Neurotrauma **40**(3–4), 318–325 (2023). https://doi.org/10.1089/neu.2022.0075
5. Stone, J.R., Avants, B.B., Tustison, N.J., Wassermann, E.M., Gill, J., Polejaeva, E., Dell, K.C., Carr, W., Yarnell, A.M., LoPresti, M.L., Walker, P., O'Brien, M., Domeisen, N., Quick, A., Modica, C.M., Hughes, J.D., Haran, F.J., Goforth, C., Ahlers, S.T.: Functional and structural neuroimaging correlates of repetitive low-level blast exposure in career breachers. J. Neurotrauma **37**(23), 2468–2481 (2020). https://doi.org/10.1089/neu.2020.7141
6. Kingery, C.N., Bulmash, G.: Air blast parameters from TNT spherical air burst and hemispherical surface burst. Technical report, US Army Armament and Development Center, Ballistic Research Laboratory (1984)
7. Federal Aviation Administration: Calculation of Safety Clear Zones for Experimental Permits Under 14 CFR §437.53(a). https://www.faa.gov/about/office_org/headquarters_offices/ast/regulations/media/Guide-Cal-of-Safety-Clear-Zones.pdf (2011). Accessed 09 Sep 2023
8. Baker, W.: Blast pressure effects: an overview. In: Scott Jr., R.A., Doemeny, L.J. (eds.) Design Considerations for Toxic Chemical and Explosives Facilities. ACS Symposium Series, vol. 345, pp. 2–57 (1987). https://doi.org/10.1021/bk-1987-0345.ch001
9. Hopkinson, B.: British Ordnance Board Minutes 13565. The National Archives, Kew (1915)
10. Cranz, C.: Lehrbuch der ballistik. Monatshefte für Mathematik und Physik **26**(1), 41–44 (1915). https://doi.org/10.1007/BF01999520
11. Swisdak, J.M.: Simplified Kingery airblast calculations. In: Proceedings of the DoD Explosives Safety Seminar (26th), Miami, FL (1994). https://ntrl.ntis.gov/NTRL/dashboard/searchResults/titleDetail/ADA526744.xhtml
12. Johnson, E.M., Grahl, N., Langenderfer, M.J., Doucet, D.P., Schott, J., Williams, K., Rutter, B., Johnson, C.: An experimental and simulated investigation into the validity of unrestricted blast wave scaling models when applied to transonic flow in complex tunnel environments. Int. J. Protect. Struct. **14**(2), 165–220 (2023). https://doi.org/10.1177/20414196221095252
13. Weibull, H.R.W.: Pressures recorded in partially closed chambers at explosion of TNT charges. Ann. N. Y. Acad. Sci. **152**(1), 357–361 (1968). https://doi.org/10.1111/j.1749-6632.1968.tb11987.x
14. Proctor, J.F.: Internal blast damage mechanisms computer program. Technical report, Naval Ordnance Lab White Oak MD (1972). https://apps.dtic.mil/sti/citations/AD0759002

15. Chernin, L., Vilnay, M., Shufrin, I., Cotsovos, D.: Pressure-impulse diagram method – a fundamental review. Proc. Inst. Civil Eng. – Eng. Comput. Mech. **172**(2), 55–69 (2019). https://doi.org/10.1680/jencm.17.00017
16. Richmond, D.R., Damon, E.G., Fletcher, E.R., Bowen, I.G., White, C.S.: The relationship between selected blast-wave parameters and the response of mammals exposed to air blast. Ann. N. Y. Acad. Sci. **152**(1), 103–121 (1968). https://doi.org/10.1111/j.1749-6632.1968.tb11970.x
17. Kamimori, G.H., LaValle, C.R., Eonta, S.E., Carr, W., Tate, C., Wang, K.K.W.: Longitudinal investigation of neurotrauma serum biomarkers, behavioral characterization, and brain imaging in soldiers following repeated low-level blast exposure (New Zealand Breacher Study). Milit. Med. **183**(suppl_1), 28–33 (2018). https://doi.org/10.1093/milmed/usx186
18. Phillips, Y.Y.: Primary blast injuries. Ann. Emerg. Med. **15**(12), 1446–1450 (1986). https://doi.org/10.1016/S0196-0644(86)80940-4
19. Ensign-Bickford Aerospace & Defense Company: PRIMASHEET®1000 Flexible Sheet Explosive Product Sheet, Simsbury, CT (2020). https://www.ebad.com/wp-content/uploads/2022/08/Primasheet-1000-Flexible-Sheet-Explosive-released-10-9-20.pdf. www.EBAD.com
20. "Ultimate," Sportfloor. https://northwestrubber.com/sportfloor/products/ultimate/. Accessed 3 Aug 2024
21. Hi-Techniques, Inc.: Synergy P Data Acquisition System, Madison, WI (2022). https://hi-techniques.com/products/synergy/p.html
22. PCB PIEZOTRONICS: PCB Model 137B23B Specifications, Depew, NY. https://www.pcb.com/products?m=137b23b (2020). Accessed 26 Oct 2022
23. PCB PIEZOTRONICS: PCB Model 102B15 Specifications. https://www.pcb.com/products?m=102b15 (2020). Accessed 26 Oct 2022
24. Belding, J.N., Egnoto, M., Englert, R.M., Fitzmaurice, S., Thomsen, C.J.: Getting on the same page: consolidating terminology to facilitate cross-disciplinary health-related blast research. Front. Neurol. **12**, 695496 (2021). https://doi.org/10.3389/fneur.2021.695496
25. BlackBox Biometrics: Wireless Blast Gauge System. https://blastgauge.com/. Accessed 26 Oct 2022
26. PCB PIEZOTRONICS: PCB Model 102B18 Specifications. https://www.pcb.com/products?m=102b18 (2022). Accessed 12 Jan 2023
27. Stoner, R.G., Bleakney, W.: The attenuation of spherical shock waves in air. J. Appl. Phys. **19**(7), 670–678 (1948). https://doi.org/10.1063/1.1698189
28. Stoner, R.G., Bleakney, W.: Erratum: The attenuation of spherical shock waves in air. J. Appl. Phys. **19**(12), 1129–1129 (1948). https://doi.org/10.1063/1.1715031
29. Cooper, P.W.: Explosive Engineering. Wiley-VCH, Albuquerque, NM (1996)
30. United States Marine Corps: Methods of Entry School, USMC, Student Handbook, 2nd edn. United States Marine Corps, Quantico, VA (2011)
31. Rutter, B., Song, H., DePalma, R.G., Hubler, G., Cui, J., Gu, Z., Johnson, C.E.: Shock wave physics as related to primary non-impact blast-induced traumatic brain injury. Mil. Med. **186**(Supplement 1), 601–609 (2021). https://doi.org/10.1093/milmed/usaa290
32. Pun, P.B., Kan, E.M., Salim, A., Li, Z., Ng, K.C., Moochhala, S.M., Ling, E.A., Tan, M.H., Lu, J.: Low level primary blast injury in rodent brain. Front. Neurol. **2**, 19 (2011). https://doi.org/10.3389/fneur.2011.00019
33. Ahlers, S., Vasserman-Stokes, E., Shaughness, M., Hall, A., Shear, D., Chavko, M., McCarron, R., Stone, J.: Assessment of the effects of acute and repeated exposure to blast overpressure in rodents: Toward a greater understanding of blast and the potential ramifications for injury in humans exposed to blast. Front. Neurol. **3**, 32 (2012). https://doi.org/10.3389/fneur.2012.00032
34. Jean, A., Nyein, M.K., Zheng, J.Q., Moore, D.F., Joannopoulos, J.D., Radovitzky, R.: An animal-to-human scaling law for blast-induced traumatic brain injury risk assessment. Proc. Natl. Acad. Sci. **111**(43), 15310–15315 (2014). https://doi.org/10.1073/pnas.1415743111
35. Reneer, D., Hisel, R., Hoffman, J., Kryscio, R., Lusk, B., Geddes, J.: A multi-mode shock tube for investigation of blast-induced traumatic brain injury. J. Neurotrauma **28**, 95–104 (2010). https://doi.org/10.1089/neu.2010.1513
36. MathWorks: Trapezoidal Numerical Integration. https://www.mathworks.com/help/matlab/ref/trapz.html. Accessed 05 May 2022
37. Thomas, C., Johnson, C.: Investigation into helmet-head shock wave interactions at low overpressures through free-field blasts and schlieren imagery. Shock Waves (2024). https://doi.org/10.1007/s00193-024-01167-4
38. Moss, W.C., King, M.J., Blackman, E.G.: Skull flexure from blast waves: a mechanism for brain injury with implications for helmet design. Phys. Rev. Lett. **103**, 108702 (2009). https://doi.org/10.1103/PhysRevLett.103.108702
39. Sarvghad-Moghaddam, H., Rezaei, A., Ziejewski, M., Karami, G.: CFD modeling of the underwash effect of military helmets as a possible mechanism for blast-induced traumatic brain injury. Comput. Methods Biomech. Biomed. Eng. **20**(1), 16–26 (2017). https://doi.org/10.1080/10255842.2016.1193597
40. Johnson, C.E.: Open Field Blast (OFB) Data Gu Lab_2019_2020. Open Data Commons for Traumatic Brain Injury. https://doi.org/10.34945/F5630G (2023). Accessed 20 Sep 2023
41. Johnson, C., Cui, J., Zuckerman, A., Song, H., Hubler, G.K., DePalma, R.G., Cernak, I., Gu, Z.: Open-field blast (OFB) model in mice. Open Data Commons for Traumatic Brain Injury. https://doi.org/10.17504/protocols.io.yxmvm2kwog3p/v1. https://www.protocols.io/view/open-field-blast-ofb-model-in-mice-yxmvm2kwog3p/v1 (2023). Accessed 20 Sep 2023
42. Chen, S., Siedhoff, H.R., Zhang, H., Liu, P., Balderrama, A., Li, R., Johnson, C., Greenlief, C.M., Koopmans, B., Hoffman, T., DePalma, R.G., Li, D.-P., Cui, J., Gu, Z.: Low-intensity blast induces acute glutamatergic hyperexcitability in mouse hippocampus leading to long-term learning deficits and altered expression of proteins involved in synaptic plasticity and serine protease inhibitors. Neurobiol. Dis. **165**, 105634 (2022). https://doi.org/10.1016/j.nbd.2022.105634
43. Belding, J.N., Englert, R., Bonkowski, J., Thomsen, C.J.: Occupational risk of low-level blast exposure and TBI-related medical diagnoses: a population-based epidemiological investigation (2005–2015). Int. J. Environ. Res. Public Health **18**(24), 12925 (2021). https://doi.org/10.3390/ijerph182412925
44. Carr, W., Stone, J.R., Walilko, T., Young, L.A., Snook, T.L., Paggi, M.E., Tsao, J.W., Jankosky, C.J., Parish, R.V., Ahlers, S.T.: Repeated low-level blast exposure: a descriptive human subjects study. Mil. Med. **181**(suppl 5), 28–39 (2016). https://doi.org/10.7205/MILMED-D-15-00137